Journal of Alloys and Compounds 681 (2016) 268–274

Contents lists available at ScienceDirect

Journal of Alloys and Compounds

journal homepage: http://www.elsevier.com/locate/jalcom

Electric Cu nanoparticles decorated V_2O_5 spheres as high performance cathodes for lithium ion batteries

Mingzhong Zou [a, b], Weiwei Wen [a, b], Jiaxin Li [a, c, *], Heng Lai [a, b], Zhigao Huang [a, b, **]

[a] College of Physics and Energy, Fujian Normal University, Fujian Provincial Key Laboratory of Quantum Manipulation and New Energy Materials, Fuzhou, 350117, China
[b] Fujian Provincial Collaborative Innovation Center for Optoelectronic Semiconductors and Efficient Devices, Xiamen, 361005, China
[c] Key Laboratory of Design and Assembly of Functional Nanostructures, Fujian Institute of Research on the Structure of Matter, Chinese Academy of Sciences, Fuzhou, 350002, Fujian, PR China

ARTICLE INFO

Article history:
Received 17 October 2015
Received in revised form
28 March 2016
Accepted 31 March 2016
Available online 4 April 2016

Keywords:
Energy storage materials
Electrode materials
Nanofabrications
Electrochemical reactions

ABSTRACT

In order to overcome the intrinsic drawbacks of V_2O_5, including the intrinsically low electrical conductivity and slow electrochemical kinetics, V_2O_5 nanospheres are uniformly mixed with the electric Cu nanoparticles for forming V_2O_5/Cu composites. As used as an cathode material for LIBs, the V_2O_5/Cu composite demonstrated obviously improved electrochemical performance including high reversible specific capacity, superior rate capability and outstanding cycling stability. The V_2O_5/Cu cathodes can afford a high reversible capacity of 186 mAh g^{-1} after 70 cycles under a current density of 300 mA g^{-1} and good rate performance. Even at a high current density of 5 A g^{-1}, a high reversible capacity of 101 mAh g^{-1} after 350 cycles can still remain. The improved performance can be contributed from the decorated Cu nanoparticles, which can result in a good contact in active materials and facilitate transportation of the electron into the inner region of the electrode.

1. Introduction

The increasing demand for high power density, high energy efficiency and good rate performance in lithium ion batteries (LIBs) has prompted extensive investigation of alternative cathode materials [1–5]. Among many cathode materials, vanadium pentoxide (V_2O_5) is a promising candidate for LIBs owing to its unique structure, high energy density, low cost and abundant source. Moreover, V_2O_5 with a typical layered crystal structure can accommodate two Li ions with a theoretical capacity of 294 mAh g^{-1}, which capacity is much higher than the capacities of more commonly used cathodes including $LiMn_2O_4$ (148 mAh g^{-1}), $LiCoO_2$ (140 mAh g^{-1}) and $LiFePO_4$ (170 mAh g^{-1}) [6–8]. However, the slow Li ion diffusion and low electronic conductivity of V_2O_5 lead to the poor cycling stability and poor rate capability. To overcome these problems and further achieve decent electrochemical performance for V_2O_5 has been a challenge.

Recently, several strategies have been used to mitigate the detrimental effects of these intrinsic drawbacks. On the one hand, fabricating nanostructured V_2O_5 materials including nanoparticles, nanocrusts and nanotubes, has been adopted to enhance their electrochemical performance [8–10]. Such strategy can effectively shorten the transport lengths of Li ions and minimize the effect of the low ionic diffusivity. For example, Ning et al. synthesized uniform V_2O_5 nanocrusts by via the combustion of a precursor by mixing commercial V_2O_5 with molten urea [9]. Wang et al. synthesized porous V_2O_5 nanotubes by a simple electrospinning technique followed by an annealing process [10]. These materials both exhibited excellent electrochemical performance, which performance was improved by their unique nanostructures. On the other hand, modifying the electrical conductivity via carbon matrix has been usually used to enhance the electrochemical performance [11–15]. In particular, the V_2O_5 cathodes with significant improvements of electrochemical performance have been achieved through synthesizing V_2O_5/carbon composite materials, such as carbon coating V_2O_5 nanosheets [11], carbon-coated V_2O_5 [12] and V_2O_5/reduced graphene [13], etc. Recently, utilization of metal nanoparticles to improve the electrical conductivity has attracted

* Corresponding author.College of Physics and Energy, Fujian Normal University, Fujian Provincial Key Laboratory of Quantum Manipulation and New Energy Materials, Fuzhou, 350117, China.
** Corresponding author. College of Physics and Energy, Fujian Normal University, Fujian Provincial Key Laboratory of Quantum Manipulation and New Energy Materials, Fuzhou, 350117, China.
E-mail addresses: 123439347@qq.com (J. Li), zghuang@fjnu.edu.cn (Z. Huang).

http://dx.doi.org/10.1016/j.jallcom.2016.03.306
0925-8388/

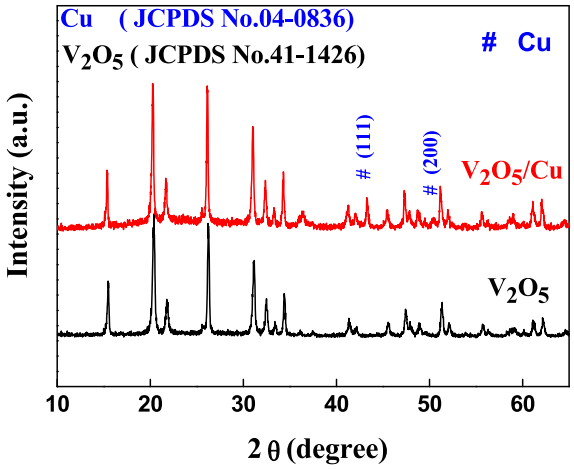

Fig. 1. XRD patterns of the V_2O_5 and V_2O_5/Cu.

extensive attention. More importantly, it is believed that metal nanoparticles possess better conductivity at low temperature than that at room temperature, thereby significantly improving their electrochemical performance at low temperature [16,17]. Recently, our group reported Ag-incorporated Fe_2O_3 carbon nanofibers (CNFs) demonstrated a much better electrochemical performance than that of pure Fe_2O_3 CNFs especially in relative low temperature. Herein, the Ag nanoparticles (NPs) can play functions in enhancing electronic conductivity [16]. Furthermore, using cheap metal of Fe or Cu also with good electrical conductivity instead of Ag is important based on the price consideration for the potential practical LIBs [17]. Considering the above mentioned advantages, it is desired to fabricate nanosized V_2O_5 cathode composites combined with dispersed cheap metal NPs with excellent conductivity.

In this work, nanostructured composites of V_2O_5 spheres decorated by electric Cu NPs (V_2O_5/Cu) have been prepared by a simple chemical reaction combined with ultrasonic mixing, and subsequently evaluated as cathodes for LIBs. The decorated Cu NPs can result in a good contact in active materials and facilitate transportation of the electron into the inner region of the electrode. As expected, the V_2O_5/Cu cathodes can afford an obviously better electrochemical performance compared to the pure V_2O_5, with a high reversible capacity of 186 mAh g^{-1} after 70 cycles under a current density of 300 mA g^{-1} and good rate performance. Even at a high current density of 5 A g^{-1}, a high reversible capacity of 101 mAh g^{-1} after 350 cycles can still remain.

2. Experimental

2.1. Material synthesis and characterization

All chemicals in experiment were of analytical grade and used as received. Typically, 6 mmol of Ammonium metavandate (NH_4VO_3)

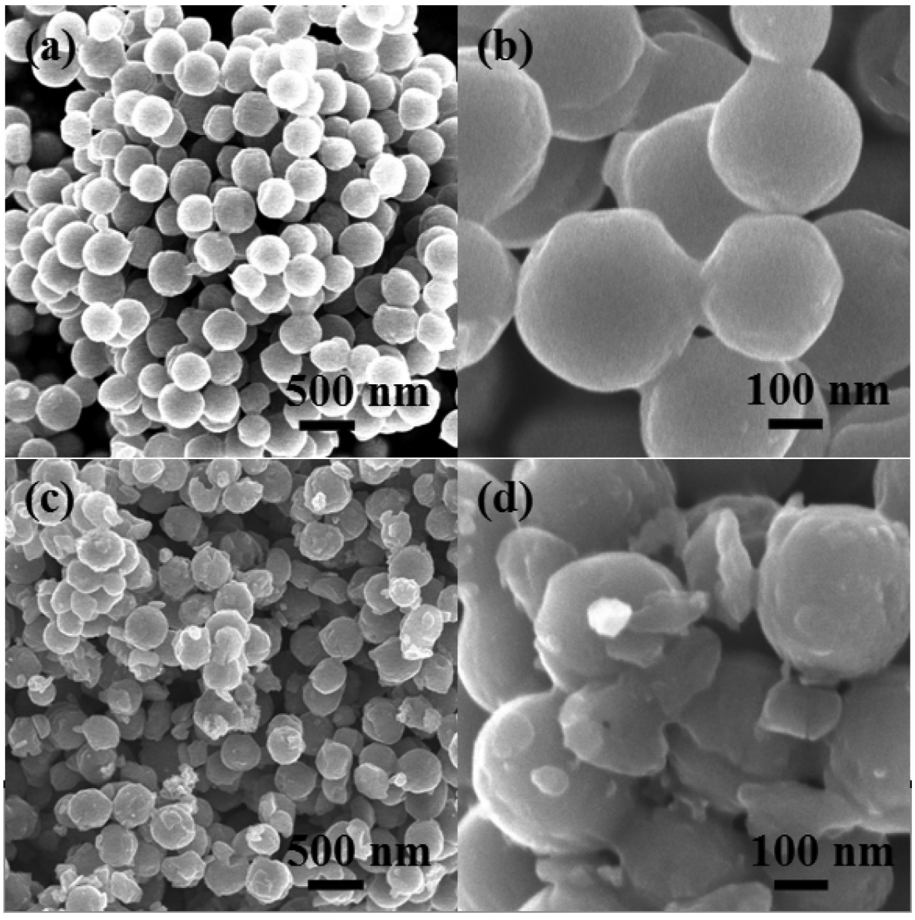

Fig. 2. SEM images of the (a,b) V_2O_5 and (c,d) V_2O_5/Cu.

was dissolved in 135 ml of de-ionized water, and solution was strongly stirred for 15 min. Then 3 ml of 1 M HCL solution was added to the solution slowly, ensuring that the solution was a transparent yellow solution. After 9 ml of hydrazine ($N_2H_4 \cdot H_2O$) was loaded into the system and strongly stirred for half a hour at room temperature, the solid precursor $V(OH)_2NH_2$ was obtained when the solution turn to gray [18,19]. The product of $V(OH)_2NH_2$ NPs was filterd and washed several times with de-ionized water, and then dried at 80 °C 12 h. The precursor was subsequently calcined at 350 °C in air for 2 h with a heating rate of 0.5 °C min^{-1} to obtain V_2O_5 NPs.

In a typical experiment, 59 mg of blue copperas and 8 mg of polyvinylpyrrolidone (PVP, M_w, 130000) was added to 15 ml de-ionized water and 10 ml of anhydrous ethanol, and the solution was sonicated for 0.5 h to form a homogeneous solution. Then, 2.5 ml $N_2H_4 \cdot H_2O$ was added to the solution drop by drop and ultrasonicated for 10 min. The product of Cu NPs was filtered and washed several times with de-ionized water, and then dried for 12 h in vacuum at 80 °C. Finally, 90 mg of V_2O_5 NPs have been mixed with 10 mg of Cu NPs in de-ionized water and sonicated for 0.5 h. The solid product was dried in vacuum at 80 °C overnight for forming the V_2O_5/Cu composites. These samples were characterized by X-ray diffraction (XRD, RIGAKU SCXmini), scanning electron microscope (SEM, JSM-6700F), transmission electron microscope (TEM, Tecnai G2 F20).

2.2. Electrode assembly and electrochemical measurements

The electrochemical behaviors were measured via CR2025 coin-type test cells assembled in a dry argon-filled glove box. The test cell consisted of working electrode (about ~1.5 mg cm^{-2}) and lithium sheet which were separated by a Celgard 2300 membrane and electrolyte of 1 M $LiPF_6$ in EC:EMC:DMC (1:1:1 in volume). The working electrode consisted of 80 *wt %* active material, 10 *wt %* acetylene black and 10 wt % polyvinylidene difluoride (PVDF). These electrochemical properties are all calculated based on the overall mass of the active material of V_2O_5 or V_2O_5/Cu. The cells were cycled by LAND2001A at room temperature. Cyclic voltammetry curves (CVs) were tested on a CHI660D Electrochemical Workstation with a scan rate of 0.5 mV s^{-1}. Electrochemical impedance measurements were carried out by applying an AC voltage of 5 mV over the frequency range from 1 mHz to 100 KHz.

3. Results and discussion

Fig. 1 shows the XRD patterns of the pure V_2O_5 and V_2O_5/Cu composites. Both of pure V_2O_5 and V_2O_5/Cu composites crystallize in a typical orthorhombic structure of V_2O_5 (JCPDS no. 41-1426). From Fig. 1, all of the diffraction peaks of the V_2O_5 around 15.3°, 20.3°, 21.7°, 26.1°, 31.0°, 32.4°, 33.3°, 34.3°, 36.0°, 41.3°, 42.0°, 45.5°, 47.3°, 48.8°, 51.2°, 52.0°, 55.6°, 61.1° and 62.1° correspond to the planes of (200), (001), (101), (110), (301), (011), (111), (310), (211), (002), (102), (411), (600), (012), (020), (601), (021), (321) and (710), respectively. Compared with the pure V_2O_5, V_2O_5/Cu presents two additional clear diffraction peaks located at 43.3° and 50.4°, which are matched well with the (111) and (200) crystal planes of Cu (JCPDS no. 04-0836). Thus, it is suggested that Cu was successfully introduced into the pure V_2O_5 for forming V_2O_5/Cu composites.

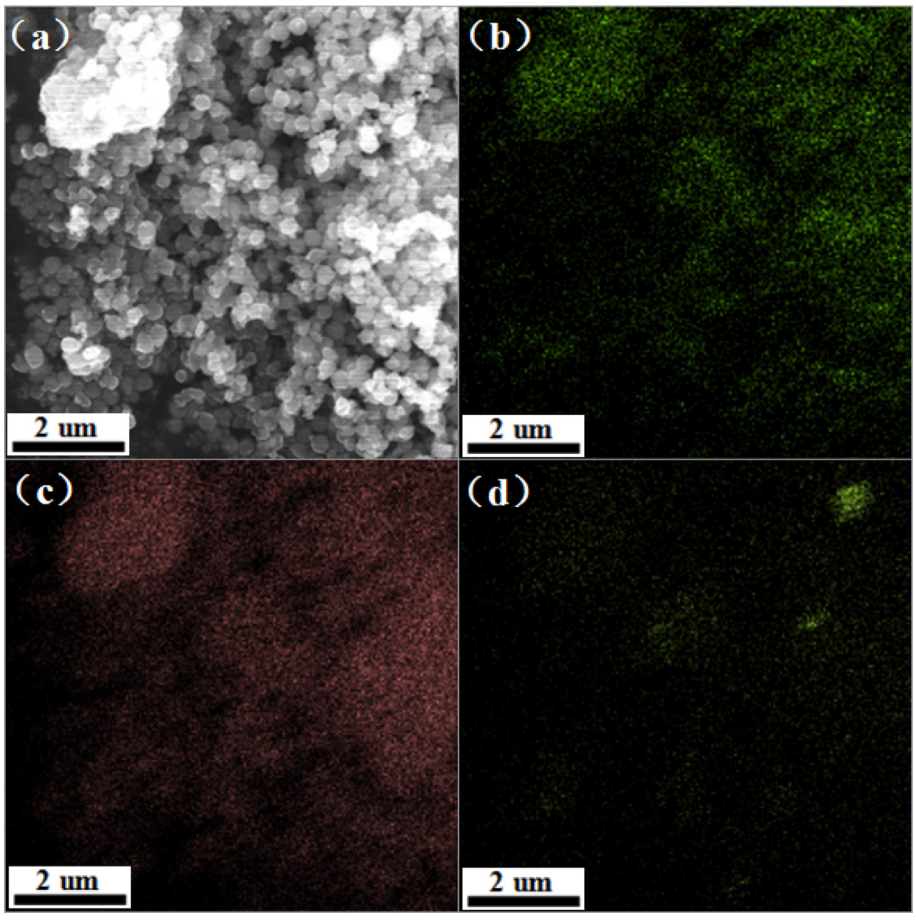

Fig. 3. (a) SEM image of V_2O_5/Cu and the corresponding EDS elemental mappings: (b) the elements of oxygen, (c) vanadium and (d) copper.

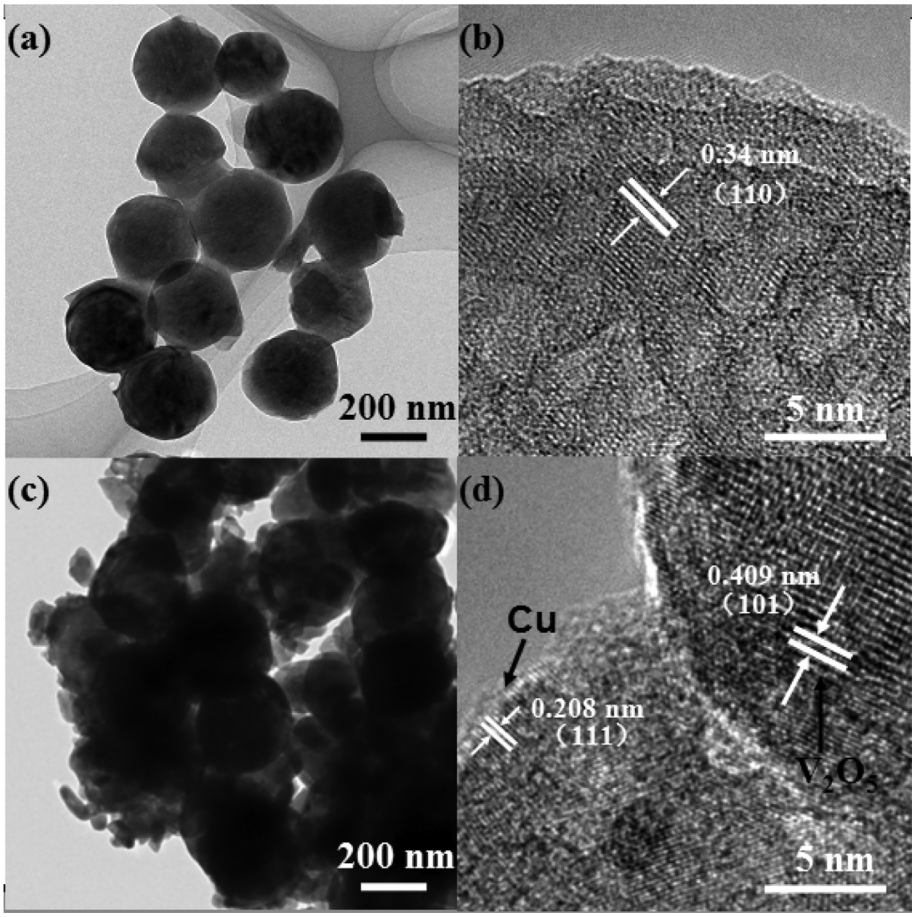

Fig. 4. TEM and HR-TEM images of the (a,b) V_2O_5 and (c,d) V_2O_5/Cu.

As shown in the Fig. 2, the morphologies of the pure V_2O_5 and V_2O_5/Cu were examined by scanning electron microscopy (SEM). From Fig. 2a and b, SEM images reveal that the pure V_2O_5 is composed of homogeneous nanospheres with diameter of about 300 nm. With the Cu nanoparticles decorating, panoramic SEM images of Fig. 2c and d displays the detailed morphologies and structure features of V_2O_5/Cu composites. It can be found that adding Cu nanoparticles does not change the general shape of V_2O_5 nanospheres but results in the difference in the surface morphology of the hybrid products. The magnified SEM image shown in Fig. 2d further reveals that Cu nanoparticles are decorated on the surface and gap of V_2O_5 nanospheres. Meanwhile, the corresponding SEM images of pure Cu nanoparticles and V_2O_5/Cu composite at similar magnification are also provided in Fig. S1. To further identify the existence of the V_2O_5/Cu, elemental acquisition at individual points and 2-dimensional mapping of V_2O_5/Cu were performed, as shown in Fig. 3. It can be seen that Cu, O and V in the sample are homogeneously distributed in the composite. These uniform Cu nanoparticles are beneficial to the fast migration of electron in the metal conductor, thereby improving their conductivity and further enhancing the electrochemical performance of these V_2O_5/Cu cathodes.

The TEM and HR-TEM images of the pure V_2O_5 and V_2O_5/Cu are given in Fig. 4 to gain insight into their microstructure. As described in Fig. 4a and c, V_2O_5 nanospheres keep the solid sphere structure with good nanocrystallites. The HR-TEM image shown in Fig. 4b reveals the interplanar spacing of 0.34 nm, corresponding to the (110) planes of V_2O_5. Meanwhile, much copper fragment scattered around the perimeter of the V_2O_5 nanospheres in the Fig. 4c. As a comparison, Fig. 4d shows the additional (111) lattice plane of Cu in the V_2O_5/Cu composites. These findings are in agreement with the SEM results.

The cyclic voltammetry (CV) curve of V_2O_5/Cu electrode at the 2nd cycle in the voltage window of 4.0–2.0 V at a scan rate of 0.5 mV s^{-1} is shown in Fig. 5a. Three distinctive peaks are shown at 3.34, 3.13 and 2.21 V versus Li/Li^+, which indicates a multistep lithium ion intercalation. Correspondingly, the phase is transformed from α-V_2O_5 to ε-$Li_{0.5}V_2O_5$ (3.34 V), δ-LiV_2O_5 (3.13 V) and γ-$Li_2V_2O_5$ (2.21 V), consecutively [10,11,13,14]. Contrarily, the anodic peaks at the potentials of 2.63, 3.28 and 3.47 V due to lithium de-intercalation signify the backward transition of phase from γ-$Li_2V_2O_5$ to δ-LiV_2O_5, ε-$Li_{0.5}V_2O_5$ and α-V_2O_5, respectively. For further comparison, the cycling stability for the first several cycles of the CVs has been demonstrated in Fig. S2a and b. Compared to the CV curves of V_2O_5, it is observed that the peaks in the following several cycles overlap well for the V_2O_5/Cu electrode, indicating that a better electrochemical reversibility. The reaction mechanism of Li^+ and V_2O_5 could be described as follows:

$$V_2O_5 + 0.5Li^+ + 0.5e^- \leftrightarrow Li_{0.5}V_2O_5 \quad (1)$$

$$Li_{0.5}V_2O_5 + 0.5Li^+ + 0.5e^- \leftrightarrow LiV_2O_5 \quad (2)$$

$$LiV_2O_5 + Li^+ + e^- \leftrightarrow Li_2V_2O_5 \quad (3)$$

Accordingly, the discharge/charge (D/C) profile of the V_2O_5/Cu electrode in the 1st, 2nd, 10th, 30th, 50th and 70th cycles at a current density of 300 mA g^{-1} between 2.0 V and 4.0 V is presented

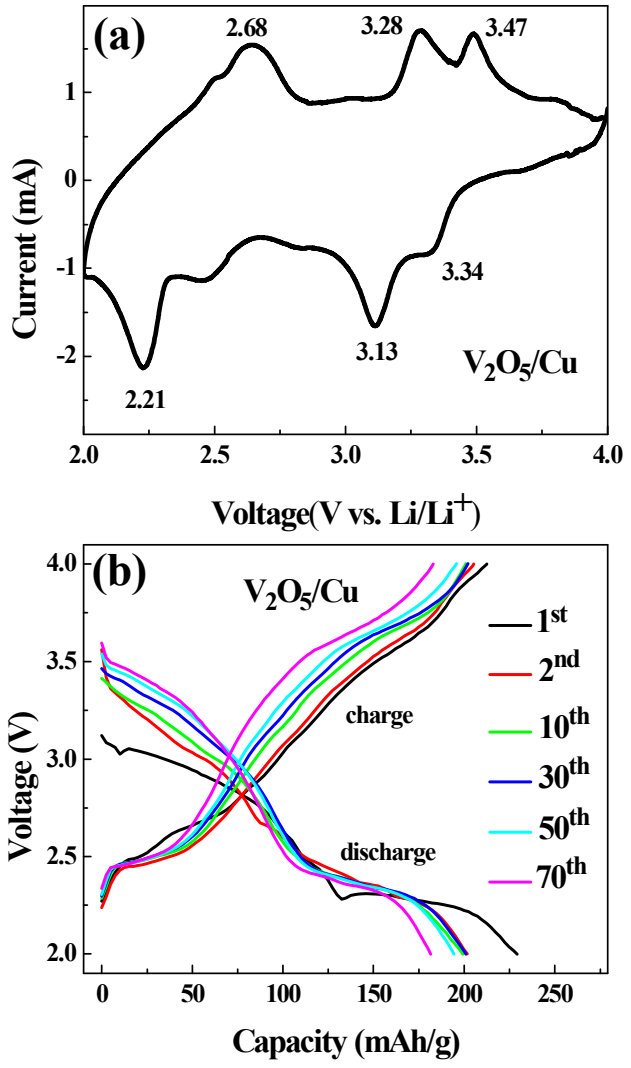

Fig. 5. (a) Cyclic voltammetry curve and (b) the 1st, 2nd, 10th, 30th, 50th and 70th discharge-charge curves between 2.0 and 4.0 V of Li insertion/extraction into/from the V_2O_5/Cu electrode.

in Fig. 5b. Those voltage plateaus shown in D/C curves for the V_2O_5/Cu electrode are consistent with the CV observation.

The comparison of cycling performance for V_2O_5 and V_2O_5/Cu electrodes at different current densities is shown in Fig. 6. Fig. 6a compares the cycling performance of these two cathodes measured at 300 mA g^{-1}. Apparently, the V_2O_5/Cu electrode exhibits a significantly improved cycling performance. After 70 cycles, the reversible capacity of V_2O_5 remained at 218 mAh g^{-1}, while that of 186 mAh g^{-1} for the V_2O_5/Cu. This result is due to the additional weight of Cu NPs calculated in the cathode active material of V_2O_5/Cu. While the cycle performances of the V_2O_5 and V_2O_5/Cu electrodes were tested at a relatively high current density of 600 mA g^{-1}, the performance changing trend is similar to those tested at 300 mA g^{-1} as shown in Fig. 6b. In order to further investigate the excellent rate capability in detail, the result for these two electrodes discharged and charged at various rates is shown in Fig. 6c. The corresponding Fig. S3 show the overlap of the voltage-capacity curves of representative circles of the two electrodes at different rates for Fig. 6c. The compared result reveals that the V_2O_5 has worse voltage polarization than V_2O_5/Cu. From Fig. 6c, the V_2O_5/Cu cathode delivered the reversible capacities of 212, 196, 180, 168, 156, 148 and 182 mAh g^{-1} at the current densities of 150, 300,

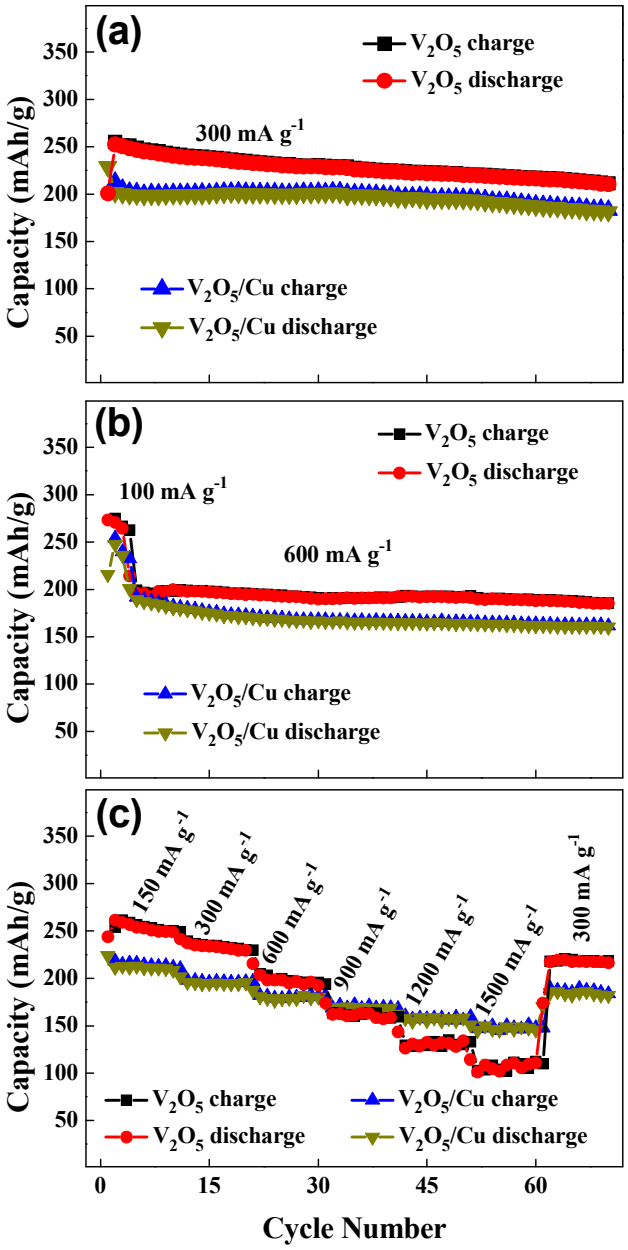

Fig. 6. Cycling performance of V_2O_5 electrode and V_2O_5/Cu electrode at room temperature: (a) at a current density of 300 mA g^{-1}; (b) at a large current density of 600 mA g^{-1} and (c) at various current rates.

600, 900, 1200, 1500 and 300 mA g^{-1}, while those of 249, 229, 193, 158, 134, 112 and 218 mAh g^{-1} for the V_2O_5. It is found that the difference of reversible capacity between two samples decrease sharply with increasing the D/C current densities. In particular, the capacities trend reversed at 900 mA g^{-1} as shown in Fig. 6c. Moreover, at a high current density of 1500 mA g^{-1}, the V_2O_5/Cu cathode delivered a capacity of 148 mAh g^{-1}, being obviously larger than that of 112 mAh g^{-1} for V_2O_5. This interesting phenomenon can be explained as follows. For Cu-incorporating cathodes, the Cu can obtain better conductivity, which can improve the electrode's interface polarization and further release the electrolyte polarization. The different polarization potentials might lead to different capacities in the relative large current densities. Therefore, it is concluded that the V_2O_5/Cu composite with Cu introducing can present an obviously improved electrochemical performance

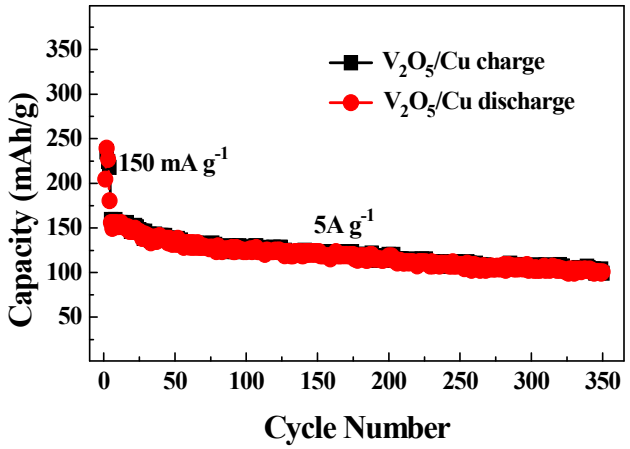

Fig. 7. Cycling performance of V_2O_5/Cu electrode at a large current density of 5 A g^{-1} at room temperature.

compared with the pure V_2O_5 electrodes. In addition, it should be noted that some electrodes exhibited the low discharged capacity at the first cycle, which may have been due to the gradual activation of electrode materials during the cycling process [20–22].

To further evaluate the long life cycle performance, the V_2O_5/Cu electrode was cycled under a relatively high current density of 5 A g^{-1}. As shown in Fig. 7, the specific reversible capacity stabilized at 101 mAh g^{-1} even after 350 cycles. Meanwhile, the coulombic efficiency of the V_2O_5/Cu electrode after the first 3 cycles kept around ~98% until 350 cycles. To the best of our knowledge, the good electrochemical performance of the V_2O_5/Cu composite, including high capacity, good cycling retention (i.e., 101 mAh g^{-1} at 5 A g^{-1} after 350 cycles), and excellent rate performance, can be comparable with the recently reports [23–28].

Electrochemical impedance spectroscopy (EIS) was performed to identify the variations of impedance in V_2O_5 and V_2O_5/Cu electrodes to further explain the improved mechanism about electrochemical performance. Fig. 8 shows EIS impedance spectra and the corresponding equivalent circuit of V_2O_5 and V_2O_5/Cu electrodes after test. It is clearly observed that the semicircle of the V_2O_5/Cu is smaller than that of the V_2O_5 electrodes. The R_{ct} (charge transfer resistance) values of V_2O_5/Cu and V_2O_5 electrode are 107 Ω and 155 Ω, respectively, indicating that the presence of Cu doping can significantly improve the charge transfer resistance, electronic conductivity and enhance kinetics of the electrode reactions.

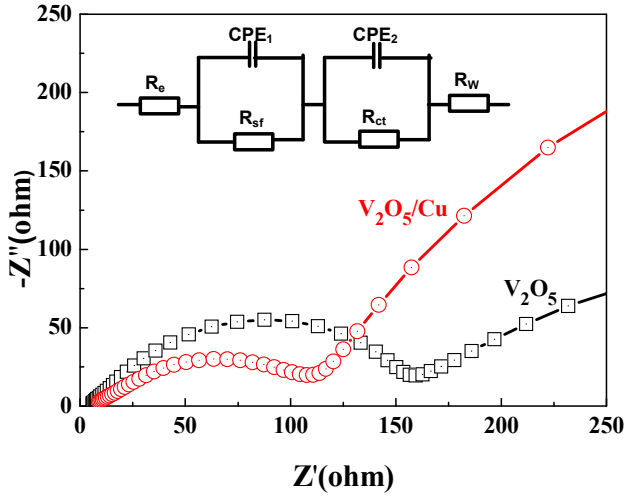

Fig. 8. The EIS profiles of V_2O_5 and V_2O_5/Cu electrodes after test. The inset shows the corresponding equivalent circuit.

4. Conclusion

In summary, a simple approach was used to fabricate V_2O_5/Cu composite in which V_2O_5 nanospheres are uniformly mixed with the electric Cu nanoparticles. As a cathode material for LIBs, the V_2O_5/Cu composite demonstrated obviously improved electrochemical performance including high reversible specific capacity, superior rate capability and outstanding cycling stability. Even at a high current density of 5 A g^{-1}, a high reversible capacity of 101 mAh g^{-1} after 350 cycles can still remain, being comparable with the recent reported results. The improved performance can be contributed from the decorated Cu NPs, which can result in a good contact in active materials and facilitate transportation of the electron into the inner region of the electrode. Furthermore, this method is proven to be an effective technique for improving the electrochemical cycling performance and stability of V_2O_5-based cathodes for LIBs.

Acknowledgements

We acknowledge the financial support by the Natural Science Foundations of China (No.21203025, No.91127020), the Strategic Priority Research Program of the Chinese Academy of Sciences (No. XDA09010400), the Science and Technology Planning Project of Fujian Province (No.2014H2008), and the National Key Project on Basic Research (Grant No. 2011CB935904).

Appendix A. Supplementary data

Supplementary data related to this article can be found at http://dx.doi.org/10.1016/j.jallcom.2016.03.306.

References

[1] R. Zhao, S. Zhang, J. Liu, J. Gu, A review of thermal performance improving methods of lithium ion battery: electrode modification and thermal management system, J. Power Sources 299 (2015) 557–577.
[2] Y. Wang, B. Liu, Q. Li, S. Cartmell, S. Ferrara, Z.D. Deng, J. Xiao, Lithium and lithium ion batteries for applications in microelectronic devices: a review, J. Power Sources 286 (2015) 330–345.
[3] D. Liu, G. Cao, Engineering nanostructured electrodes and fabrication of film electrodes for efficient lithium ion intercalation, Energy Environ. Sci. 3 (2010) 1218.
[4] R. Marom, S.F. Amalraj, N. Leifer, D. Jacob, D. Aurbach, A review of advanced and practical lithium battery materials, J. Mater. Chem. 21 (2011) 9938–9954.
[5] J. Li, Y. Zhao, N. Wang, Y. Ding, L. Guan, Enhanced performance of a MnO_2–graphene sheet cathode for lithium ion batteries using sodium alginate as a binder, J. Mater. Chem. 22 (2012) 13002.
[6] H. Zhao, A. Yuan, B. Liu, S. Xing, X. Wu, J. Xu, High cyclic performance of V_2O_5@PPy composite as cathode of recharged lithium batteries, J. Appl. Electrochem. 42 (2012) 139–144.
[7] D. Pham-Cong, K. Ahn, S.W. Hong, S.Y. Jeong, J.H. Choi, C.H. Doh, J.S. Jin, Cathodic performance of V_2O_5 nanowires and reduced graphene oxide composites for lithium ion batteries, Curr. Appl. Phys. 14 (2014) 215–221.
[8] K. Zhu, Y. Meng, H. Qiu, Y. Gao, C. Wang, F. Du, Y. Wei, G. chen, Facile synthesis of V_2O_5 nanoparticles as a capable cathode for high energy lithium-ion batteries, J. Alloys Compd. 650 (2015) 370–373.
[9] Q. Song, H. Pang, W. Gong, G. Ning, S. Gao, X. Dong, C. Liu, J. Tian, Y. Lin, Fabrication of nanostructured V_2O_5 via urea combustion for high-performance Li-ion battery cathode, RSC Adv. 5 (2015) 4256–4260.
[10] Z. Li, G. Liu, M. Guo, L. Ding, S. Wang, H. Wang, Electrospun porous vanadium pentoxide nanotubes as a high-performance cathode material for lithium-ion batteries, Electrochimica Acta 173 (2015) 131–138.
[11] Y. Xu, M. Dunwell, L. Fei, E. Fu, Q. Lin, B. Patterson, B. Yuan, S. Deng, P. Andersen, H. Luo, G. Zou, Two-dimensional V_2O_5 sheet network as electrode for lithium-ion batteries, ACS Appl. Mater. Interfaces 6 (2014) 20408–20413.
[12] M. Ihsan, Q. Meng, L. Li, D. Li, H. Wang, K.H. Seng, Z. Chen, S.J. Kennedy, Z. Guo, H.-K. Liu, V_2O_5/mesoporous carbon composite as a cathode material for lithium-ion batteries, Electrochimica Acta 173 (2015) 172–177.

[13] Y. Yang, L. Li, H. Fei, Z. Peng, G. Ruan, J. Tour, Graphene nanoribbon/V_2O_5 cathodes in lithium-ion batteries, ACS Appl. Mater. Interfaces 6 (2014) 9590–9594.
[14] B. Sun, K. Huang, X. Qi, X. Wei, J. Zhong, Rational construction of a functionalized V_2O_5 nanosphere/MWCNT layer-by-layer nanoarchitecture as cathode for enhanced performance of lithium-ion batteries, Adv. Funct. Mater. 25 (2015) 5633–5639.
[15] J. Shin, H. Jung, Y. Kim, J. Kim, Carbon-coated V_2O_5 nanoparticles with enhanced electrochemical performance as a cathode material for lithium ion batteries, J. Alloys Compd. 589 (2014) 322–329.
[16] M. Zou, J. Li, W. Wen, L. Chen, L. Guan, H. Lai, Z. Huang, Silver-incorporated composites of Fe_2O_3 carbon nanofibers as anodes for high-performance lithium batteries, J. Power Sources 270 (2014) 468–474.
[17] J. Li, W. Wen, G. Xu, M. Zou, Z. Huang, L. Guan, Fe-added Fe_3C carbon nanofibers as anode for Li ion batteries with excellent low-temperature performance, Electrochimica Acta 153 (2015) 300–305.
[18] J. Shao, X. Li, Z. Wan, L. Zhang, Y. Ding, Q. Qu, H. Zheng, Low-cost synthesis of hierarchical V2O5 microspheres as high-performance cathode for lithium-ion batteries, ACS Appl. Mater. interfaces 5 (2013) 7671–7675.
[19] C. Wu, X. Zhang, B. Ning, J. Yang, Y. Xie, Shape evolution of new-phased lepidocrocite VOOH from single-shelled to double-shelled hollow nanospheres on the basis of programmed reaction-temperature strategy, Inorg. Chem. 48 (2009) 6044–6054.
[20] H.G. Wang, D.L. Ma, Y. Huang, X.B. Zhang, Electrospun V2O5 nanostructures with controllable morphology as high-performance cathode materials for lithium-ion batteries, Chemistry 18 (2012) 8987–8993.
[21] H. Song, C. Zhang, Y. Liu, C. Liu, X. Nan, G. Cao, Facile synthesis of mesoporous V2O5 nanosheets with superior rate capability and excellent cycling stability for lithium ion batteries, J. Power Sources 294 (2015) 1–7.
[22] Y. Liu, E. Uchaker, N. Zhou, J. Li, Q. Zhang, G. Cao, Facile synthesis of nanostructured vanadium oxide as cathode materials for efficient Li-ion batteries, J. Mater. Chem. 22 (2012) 24439.
[23] M. Chen, X. Xia, J. Yuan, J. Yin, Q. Chen, Free-standing three-dimensional continuous multilayer V_2O_5 hollow sphere arrays as high-performance cathode for lithium batteries, J. Power Sources 288 (2015) 145–149.
[24] Y. Dong, H. Wei, W. Liu, W. Zhang, Y. Yang, Template-free synthesis of V_2O_5 hierarchical nanosheet-assembled microspheres with excellent cycling stability, J. Power Sources 285 (2015) 538–542.
[25] S. Lin, B. Shao, I. Taniguchi, One-step synthesis of dense and spherical nanostructured V_2O_5 particles for cathode of lithium batteries and their electrochemical properties, Mater. Res. Bull. 49 (2014) 291–295.
[26] M.M. Rahman, A.Z. Sadek, I. Sultana, X.J. Dai, M.R. Field, D.G. McCulloch, S.B. Ponraj, Y. Chen, Self-assembled V_2O_5 interconnected microspheres produced in a fish-water electrolyte medium as a highperformance lithium-ion-battery cathode, Nano Res. 8 (2015) 3591–3603.
[27] D.W. Su, S.X. Dou, G.X. Wang, Hierarchical orthorhombic V_2O_5 hollow nanospheres as high performance cathode materials for sodium-ion batteries, J. Mater. Chem. A 2 (2014) 11185–11194.
[28] L. Mai, Q. An, Q. Wei, J. Fei, P. Zhang, X. Xu, Y. Zhao, M. Yan, W. Wen, L. Xu, Nanoflakes-assembled three-dimensional hollow-porous V_2O_5 as lithium storage cathodes with high-rate capacity, Small 10 (2014) 3032–3037.